BROOKHAVEN
NATIONAL LABORATORY

BNL-108288-2015-JA

Resistance of Fly Ash-Portland Cement Blends to Thermal Shock

Tatiana Pyatina and Toshifumi Sugama

Submitted to Advances in Cement Research Journal

August 2015

Sustainable Energy Technologies Department

Brookhaven National Laboratory

US DOE Office of Energy Efficiency and Renewable Energy

Notice: This manuscript has been authored by employees of Brookhaven Science Associates, LLC under Contract No. DE-AC02-98CH10886 with the U.S. Department of Energy. The publisher by accepting the manuscript for publication acknowledges that the United States Government retains a non-exclusive, paid-up, irrevocable, world-wide license to publish or reproduce the published form of this manuscript, or allow others to do so, for United States Government purposes.

This preprint is intended for publication in a journal or proceedings. Since changes may be made before publication, it may not be cited or reproduced without the author's permission.

DISCLAIMER

This report was prepared as an account of work sponsored by an agency of the United States Government. Neither the United States Government nor any agency thereof, nor any of their employees, nor any of their contractors, subcontractors, or their employees, makes any warranty, express or implied, or assumes any legal liability or responsibility for the accuracy, completeness, or any third party's use or the results of such use of any information, apparatus, product, or process disclosed, or represents that its use would not infringe privately owned rights. Reference herein to any specific commercial product, process, or service by trade name, trademark, manufacturer, or otherwise, does not necessarily constitute or imply its endorsement, recommendation, or favoring by the United States Government or any agency thereof or its contractors or subcontractors. The views and opinions of authors expressed herein do not necessarily state or reflect those of the United States Government or any agency thereof.

Main Text
Click here to download Main Text: Pyatina-Resistance of Class F fly ash-OPCad system to thermal shock.docx

March 9, 2015

4799 words; 5 figures

Resistance of Fly Ash-Portland cement blends to thermal shock

Tatiana Pyatina

Sustainable Energy Technologies, Brookhaven National Laboratory, Upton, USA

Toshifumi Sugama

Sustainable Energy Technologies, Brookhaven National Laboratory, Upton, USA

Corresponding author: Tatiana Pyatina, tpyatina@bnl.gov; Building 734, Brookhaven Ave., Upton, NY 11973-5000

Abstract
Thermal-shock resistance of high-content fly ash-Portland cement blends was tested in the following ways. Activated and non-activated blends with 80-90 % fly ash F (FAF) were left to set at room temperature, then hydrated for 24 hours at 85°C and 24-more hours at 300°C and tested in five thermal-shock cycles (600°C heat – 25°C water quenching). XRD, and thermal gravimetric analyses, along with calorimetric measurements and SEM-EDX tests demonstrated that the activated blends form more hydrates after 24 hours at 300°C, and achieve a higher short-term compressive strength than do non-activated ones. Sodium meta-silicate and soda-ash engendered the concomitant hydration of OPC and FAF, with the formation of mixed crystalline FAF-OPC hydrates and FAF hydrates, such as garranite, analcime, and wairakite, along with the amorphous FAF hydration products. In SS-activated and non-activated blends separate OPC (tobermorite) and FAF (amorphous gel) hydrates with no mixed crystalline products formed. The compressive strength of all tested blends decreased by nearly 50% after 5 thermal-shock test cycles. These changes in the compressive strength were accompanied by a marked decrease in the intensities of XRD patterns of the crystalline hydrates after the thermal-shock. There was no significant difference in the performance of the blends with different activators.
Keywords: materials technology, energy, renewable energy, drilling and drill holes
List of abbreviations:
FAF – fly ash F
OPC- ordinary Portland cement
SMS – sodium meta-silicate
SA – soda ash
SS – sodium sulfate

1. Introduction

One of the challenges in ensuring the integrity of geothermal wells is the stability of the cement sheath under conditions of thermal shock when wells, constructed under relatively mild temperatures of about 80 to 100°C, are moved into production, and the temperature may rise by several hundred degrees. Differences in temperature between the injection- and production-heat-carrier fluids may further impose a constant thermal-shock on the cement. In enhanced geothermal systems, the cement experiences an additional thermal stress during the stimulation process when large volumes of cold water are injected through the hot wells to create a connected network of fractures to make the wells more economical. To withstand such stress, the cement must be resistant to thermal shock and thermal-cycle fatigue.

Previous work (Gill *et al.*, 2012) focused on investigating the effectiveness of sodium metasilicate-activated fly ash, class F (FAF, siliceous fly ash) in improving the thermal shock resistance of Al_2O_3-rich refractory calcium aluminate cement (RCAC). RCAC consists of three crystalline phases, corundum (α-Al_2O_3), calcium monoaluminate ($CaO.Al_2O_3$, CA), and calcium dialuminate ($CaO.2Al_2O_3$, CA_2). Accelerated thermal-shock-resistance tests, wherein cement cured for 24 hours at 200°C under the pressure of 6.89 MPa was sintered at 500°C for 24 more hours, and subsequently quenched in 25°C water, showed that this cement withstands 5-cycles

of thermal shock without any failure in its integrity, such as visual cracks, partial surface spalling, or disintegration. Further, this cement showed no significant change in compressive strength, maintaining a strength of more than 6.89 MPa. Analyses of its phase composition demonstrated that after autoclaving at 200°C, four crystalline products formed in the cement, boehmite and katoite from the RCAC, hydrogrossular by the interaction between RCAC and FAF, and hydroxysodalite from FAF. After thermal-shock testing, three crystalline phase-transformations occurred: 1) boehmite $\rightarrow$ γ-Al_2O_3, 2) katoite $\rightarrow$ calcite, and 3) hydroxysodalite $\rightarrow$ carbonated sodalite. Thus, these three phases, γ-Al_2O_3, calcite from RCAC, and carbonated sodalite from FAF, maintained the integrity of the cementitious structure, and sustained the material's compressive strength developed after the autoclaving. RCAC improved the resistance of the FAF to the thermal shock.

Fly ash is a very attractive material for using in cement due to its wide availability, good workability, and compatibility with various cementitious materials. Replacing Ordinary Portland Cement (OPC) by fly ash also helps to abate CO_2 emissions during the production of the cement. However, the reactivity of FAF at temperatures below 90°C generally is low so it is very difficult to assemble an ideal cementitious structure along with a desirable strength at the early curing ages (Feldman *et al.*, 1990; Berry *et al.*, 1990; Lam *et al.*, 2000; Gurney *et al.*, 2012). There are two ways to deal with this issue. One is to incorporate it into the cementitious reactants, such as OPC, PC clinker, gypsum, or lime, which can form ettringite (AFt, $Ca_6Al_2(SO_4)_3(OH)_{12}.26H_2O$), monosulfate (AFm, $Ca_4Al_2O_6(SO_4).14H_2O$), calcium silicate hydrate ($CaO\text{-}SiO_2\text{-}H_2O$) and portlandite ($Ca(OH)_2$), along with the alkaline activators, like sodium silicate made with various Na_2O/SiO_2 mole ratios, NaOH, KOH, $Ca(OH)_2$, Na_2CO_3, Na_2SO_4 alone or in combination (Shi *et al.*, 1995; Bentz and Ferraris, 2010; Duran-Herrera *et al.*, 2011; Pacewska and Wilinska, 2013; Donatello *et al.*, 2013). The other way to increase FAF reactivity is to incorporate only alkaline activators without any additional cementitious reactants (Davidovits 1991; Palomo *et al.*, 1999; van Jaarsveld *et al.*, 2002; Fernandez-Jimenez and Palomo, 2005; Komnitsas and Zaharaki, 2007; Andini *et al.*, 2008; Mandal and Majumdar, 2009; Lohani *et al.*, 2012; Joshi and Kadu, 2012; Rodriguez *et al.*, 2013; Chi and Huang, 2013).

In FAF blends with other cementitious materials, the FAF initially serves as a filler, densifying, and thus strengthening, the structure of faster reacting cementitious phases at the early curing stages. Subsequently, the dissolution of FAF by the alkaline activators, followed by pozzolanic reactions, causes the formation of a secondary binding phase, an amorphous Na_2O -, $CaO\text{-}Al_2O_3\text{-}SiO_2\text{-}H_2O$ gel (Berry et al., 1990; Fraay *et al.*, 1989; Ben Haha *et al.*, 2010; Deschner *et al.*, 2012). The early reaction of cementitious materials assures the early development of strength. In the RCAC/FAF system, RCAC plays that role. As for the OPC-FAF blends, the combined systems of OPC and FAF had better thermal stability (Gill *et al.*, 2012; Donatello *et al.*, 2014) and resistance to acid (Donatello *et al.*, 2013), compared with those of OPC alone.

In exploring the activation of alkaline fly ash, most of the work has been done with 100 % FAF. Very high OH^- concentrations in solutions of alkaline activators, such as NaOH and/or Na-or K-silicate promote the dissolution of FAF. Thereafter, the interactions between dissociated ionic species, such as $Al(OH)^{4-}$, H_3SiO^{4-}, Na^+, and K^+, take place within the assemblage of hydroxylated Na-, and K,-aluminosilicate gel. Finally, dehydroxylation-polycondensation reactions between the hydroxylated aluminosilicates result in a three-dimensional amorphous aluminosilicare network (Davidovits, 1991; Komnitsas and Zaharaki, 2007) that contributes to the development

of early strength, and offers an excellent resistance to acid (Bakharev, 2005) and to high heat temperatures (Bakharev, 2006; Bignozzi et al., 2014). FAF-rich alkali-activated cements appear to possess an adequate resistance to both the high heat followed by water quenching thermal shock, and high-temperature sintering environments.

For geothermal wells wherein the bottom-hole temperature may reach 300°C at pressures of 8.3 MPa, the resistance of FAF-reach OPC blends with different activators cured at 300°C to thermal shock cycles is of particular interest. This study focused on the resistance of 80/20- and 90/10-wt.% FAF/OPC blends activated by three different Na- alkaline activators, viz., sodium silicate, sodium carbonate, and sodium sulfate, to thermal-shock cycles. For comparison, non-activated FAF-rich OPC systems with the same mass-component ratios also were studied. The work addressed the following four major subjects: 1) characterizing the effect of these alkaline activators on the cements' setting behaviors by measuring the amount of heat released during blends' hydration; 2) identifying the crystalline- and amorphous-phases formed in 300°C-autoclaved cements; 3) investigating the transformation of these phases after thermal-shock tests; and, 4) exploring the microstructure developed in autoclaved cements and its alteration after the thermal-shock tests. This microstructural information is correlated with the changes in compressive strength after thermal-shock testing. To conduct accelerated tests a considerable thermal stress was imposed on cement. The multiple heat-water quenching cycle procedure was performed under an extremely large temperature difference between heating the cement at 600°C and water quenching it at 25°C.

2. Experimental procedures

The effect of three Na-alkaline activators, sodium metasilicate (SMS) anhydrous, soda ash (SA) or sodium carbonate anhydrous, and sodium sulfate (SS) anhydrous, on changes in cement's integrity during repeated thermal shock was evaluated. The 93% SMS-beaded powder under the trade name "MetsoBeads 2048," was supplied by the PQ Corporation; it had a 50.5/46.6 Na_2O/SiO_2 weight ratio. The particle size of this beaded powder ranged from 0.23- to 0.85-mm. The 99.8% "soda ash light" supplied by BRI-CHEM Corp. had the following distribution of particle size in weight percent: 88 % - 0.15 mm, 8.% - 0.45 mm, 2% - 0.075 mm, and 1% - 0.6 mm. Sodium sulfate of more than 99.9% purity was obtained from Sigma-Aldrich. Boral Material Technologies, Inc. supplied Class F fly ash and White Cap Construction Supply Inc. provided type II Ordinary Portland Cement. Table 1 gives the chemical compositions of these cement-forming materials detected by energy-dispersive X-ray spectrometer (EDX), along with the composition of the sodium metasilicate activator. The X-ray powder diffraction (XRD) data showed three major crystalline phases in FAF: quartz (SiO_2), mullite ($3Al_2O_3.2SiO_2$), and hematite (Fe_2O_3).

The cementitious blends had FAF/OPC weight ratios of 80/20 and 90/10. Activators were added at 6.2% by the total weight of the blend to make the dry mixtures. The cement slurries were prepared by adding an appropriate amount of water to these mixtures. The water/cement ratio ranged from 0.44 to 0.45. After thoroughly hand-mixing the cement slurries for 1 min, samples were cast in cylindrical molds (20 mm diam. and 40 mm long), and left to harden for 24 hours at room temperature. Then, the hardened cements were placed for 24 hours into an oven at relative humidity >95% and temperature of 85°C. Next, they were autoclaved at 300°C under a

pressure of 8.3 MPa for another 24 hours. To obtain information on their thermal-shock resistance, a multiple heating-water quenching cycle test was conducted. Namely, in one cycle, the 300°C-autoclaved cements were placed in an air oven at 600°C for 24 hours, and then these heated cements were rapidly immersed in water at 25°C. This 600°C heating → water quenching cycle was repeated five times.

After assessing the strength of the specimens, they were ground into a very fine powder and dried at 90°C for 24 hours before thermogravimetric testing and X-ray diffractometric characterization. The former analysis was done on approximately 10 mg of a sample heated at a rate of 20°C/min in N_2, using TGA-Q50 from TA Instruments. The samples were examined using a Philips XRG 300 X-ray diffractometer with a 40 kV, 40 mA copper anode X-ray tube. The results were analyzed using the PDF-4/Minerals 2013 database of International Center for Diffraction Data. The morphologies of the cements were explored on typical spots of freshly fractured samples with a JEOL 7600F scanning electron microscope equipped with an EDX Oxford Link microanalysis system. The specimens were placed on metallic holders and chromium-coated. The hydration behavior of the blends was studied using isothermal calorimetry at 25°C. The slurries were mixed by hand poured into ampules and placed into the calorimeter to follow evolving heat for several days.

3. Results and discussion

3.1. Hydration behavior of FAF/OPC blends with different activators at 25°C – calorimetric measurements

Figure 1 shows the calorimetric curves of hydration heat for 80/20 weight ratio FAF/OPC blends with and without activators at 25°C. The beginning of the heat release in non-activated and SS-activated blends took longer (4 hours 42 minutes and 3 hours 18 minutes, respectively) than in the blends with SMS- and SS-activators (immediate heat release for the SMS-activated one, and 50 minutes-delay in the SA-activated one). Importantly, most of the heat was released with high intensity in a short time of about 8 hours for the last two blends while non-activated- and SS-activated blends released their heat in wide strongly or partially overlapping peaks over several days. Although each heat peak likely corresponds to a combination of the events of wetting, dissolution, alkaline activation and hydrate formation, it is likely that in the non-activated blend, the OPC, which is more reactive, starts hydrating before the FAF, which is activated later by the OPC hydration products. As a result the initial OPC hydration and formation of the first hydrates takes place as would be expected for the OPC hydrating alone. Among the activated blends, only the one with the SS-activator had well-separated peaks of heat release, while, for the SMS- and SA-activated blends all exothermic reactions were clearly much more concurrent, resulting in merged peaks. The integrated heat release was the highest for the SS-activated blend (37.5 J/g of slurry). The non-activated, SMS- and SA-activated blends released similar amount of heat (32.7, 30.4 and 31.6 J/g of slurry, respectively). It is likely that in the case of the SMS-activated blend, part of the heat was released before the instrument re-equilibrated after the ampules introduction and hence, was not registered, resulting in underestimating the actual total heat value.

In summary the results suggest that, without an activator, the blend hydrated in two somewhat separate stages with the cement hydrating first; but, in the presence of the activators the hydration of cement and fly ash pozzolanic reactions occurred simultaneously.

3.2. Compressive strength

Table 2 shows the compressive strength of 300°C-autoclaved non-activated, and SMS-, SA-, and SS-activated 80/20 and 90/10 weight ratio FAF/OPC cements before and after thermal shock testing. For the non-activated cements, the 80/20 and 90/10 ratio samples before testing had compressive strength of 16.5 and 8.9 MPa, respectively. These values increased in activated cements and the increase was more dramatic for the blends with the higher FAF content (90/10 FAF/OPC), which could be explained by higher contribution of the activated FAF to the strength. For the 80/20 FAF/OPC blends the compressive strength increase was 22-, 16-, and 4-% , respectively, for the SS-, SMS-, and SA-activators , while for the 90/10 blends the respective increases in compressive strength were 55-, 38-, and 34-%. Among the activators, SS conferred the highest compressive strength and SA the lowest.

Three samples of each non-activated and activated blend were tested in thermal-shock tests. Two out of three samples of the non-activated 80/20 OPC/FAF blend developed multiple cracks and disintegrated after the annealing in an oven at 600°C. Consequently, the 5-cycle thermal-shock tests and compressive strength measurements were performed only on one sample.

In contrast, there were no visual cracks on the 90/10 ratio cement after heating at 600°C. The strength of all samples fell after the thermal-shock tests. For the non-activated samples it declined by 46% and 52% for the 80/20 and 90/10 ratios, respectively. The decline in strength was similar for all activated 80/20 ratio samples; it varied from 46- to 49-%. In the case of the 90/10 ratio blends, the SS-activated cement revealed the lowest reduction in strength of 34%, while it was 51% and 60% for SMS and SA, respectively.

In summary, all activators improved the compressive strength of non-activated blends. The strength dropped for all the blends by more than 40-50% after 5 thermal shock cycles.

3.3. Changes in crystalline phase composition after thermal shock (XRD)

Figure 2 compares XRD data of non-heated 80/20 ratio FAF/OPC samples against those of the samples exposed to five thermal shock cycles. Table 3 summarizes the crystalline composition of 80/20 ratio FAF/OPC blends.

After the 300°C hydration and before the thermal shock tests, all the patterns revealed the peaks of non-reacted FAF phases, such as quartz, mullite, and hematite. In addition, the non-activated blend had peaks of the OPC reaction product, tobermorite (characteristic peak at 7.8° 2Θ). There also was a wide peak between 12 and 14° 2Θ on this pattern, possibly from poorly crystalized CSH(I). The peaks for tobermorite also were present in the pattern of the SS activated blend. The Sieve fitting program suggested the possible presence of riversideite (tobermorite 9A) in the SMS-activated sample. This phase generated a small peak that did not overlap with any other phase at 28.2° 2Θ. The formation of the OPC reaction products suggests a faster OPC than FAF hydration and hydrates crystallization in the non-activated and SS-activated blends, which also was suggested by the calorimetric measurements. The sodium-

sulfate-activated blend revealed anhydrate peak (2Θ-25.6°) at both the FAF/OPC ratios. The intensity of this peak was 37% higher for the 90/10 blend (data not shown) than for the 80/20 FAF/OPC blend. At the same time, calcite, identified in all other samples, was absent in the 90/10 FAF/OPC sodium-sulfate-activated blend (main peak at 2Θ-29.5°), indicating a possible reaction between calcite originally present in the OPC with the SS activator and/or the reaction of calcium ions released during the cement hydration with the sulfate ions from the activator. Although there were more crystalline products formed in the blend with SA activator, there was no tobermorite among them. Competition from carbonate anions for calcium cations could be a possible reason for this lack. The pattern of this sample showed the most intense calcite peaks. FAF hydrate analcime (aluminum sodium silicate hydrate) was identified in the XRD patterns of blends with SMS and SA activators. The presence of wairakite (sodium calcium aluminum silicate hydrate) cannot be excluded; however, its peaks overlap with those of analcime so its identification was problematic. SMS-activated- blend patterns had weak peaks while SA-activated blend ones had strong peaks of garronite (sodium calcium aluminum silicate hydrate). Garronite forms from the aluminum and silicon that mostly are supplied by FAF, sodium, which comes mostly from the activators, and calcium ions released during the OPC hydration. Intense garronite peaks in the patterns of the blend activated with SA support the concurrent hydration of OPC and FAF that was indicated by the merged high-intensity hydration heat peak in the calorimetric tests. The SMS, on the other hand, is a known accelerator of the cement hydration. Although it activates FAF, it is likely that OPC hydration happens faster, so accounting for the crystallization of OPC hydration products. The co-existence of tobermorite and Ca-containing zeolites is interesting; zeolites are believed to form from the amorphous gel that precipitates as the initial hydration product of FAF dissolution (Fernandez-Jimenez and Palomo, 2005). As an alternative to concurrent OPC and FAF hydration, it also is possible that garronite forms with calcium supplied by the OPC-hydration products that become unstable later under the experimental conditions. There were no portlandite peaks in any of the XRD patterns. Portlandite was shown to be unstable under conditions of thermal shock, decomposing with the formation of free lime and the re-crystallization of portlandite when exposed to water, so damaging the matrix (Gill *et al.*, 2012). Hence, the absence of portlandite in the OPC/FAF blends was a desirable feature.

The glassy amorphous halo between 18 and 35° 2Θ was present in all the hydrated samples. Both amorphous hydration products and glassy phases originally present in the fly ash contribute to this halo (Donatello *et al.*, 2014). Since the same fly ash was used for all the blends and its lower reactivity in the case of SMS is unlikely, it is reasonable to conclude that the SMS-activated blend with the largest halo contained the largest amount of the amorphous hydration products, while SA-activated blend with the smallest halo had the least, forming mostly crystalline hydrates. In all the cases, the halo slightly increased after the thermal shock while the peak intensities of crystalline phases either decreased or disappeared.

Thus, the intensity of tobermorite peaks was reduced in non-activated-and SS-activated- blends and had disappeared from the patterns of the SMS-activated one. The intensities of the analcime- and garronite-peaks significantly declined, suggesting their decomposition or transition to a poorly crystallized state. Finally, goethite and sillimanite possibly were present in the blend without activators; however it was difficult to confirm this because of the overlapping patterns.

3.4. FT-IR study

The spectrum for the original FAF (not shown) included four absorption bands: at 1035- and 776-cm^{-1} due to the M-O (M: Si or Al) asymmetric (V_{as} M-O), and symmetric (V_s M-O) stretching vibrations, respectively, in M-O-Si linkages, (Kline and Mullins, 1991; Uchino *et al.*, 1991; Bakharev, 2005). The bands at 792- and 694-cm^{-1} were attributed, respectively, to Si-O symmetric stretching (V_s Si-O) and Si-O bending ($\delta_{O\text{-}Si\text{-}O}$) vibrations in quartz (Saikia *et al.*, 2008; Ramasamy and Suresh, 2009). Type II OPC revealed bands at 1621 cm^{-1} related to the H-O-H bending ($\delta_{H\text{-}O\text{-}H}$), at 1445 and 847 cm^{-1} associated with C-O asymmetric stretching (V_{as} C-O), and O-C-O bending ($\delta_{O\text{-}C\text{-}O}$) in carbonate CO_3^{2-} (Xyla and Koutsoukos, 1989; Gunasekaran *et al.*, 2006; Ylmen and Jaglid, 2013), whilst the bands at 1140 and 662 cm^{-1} belonged to the S-O symmetric stretching ($V_{s\ S\text{-}O}$) and O-S-O bending ($\delta_{o\text{-}s\text{-}o}$) of SO_4^{2-} in gypsum (Garcia-Lodeiro *et al.*, 2011); all the rest of the bands could be associated with calcium-silicate, -aluminate, and –aluminoferrite anhydrous compounds (Ghosh and Handoo, 1980).

In comparison with the original FAF- and OPC-spectra, after autoclaving the FAF/OPC blends at 300°C, the $V_{as\ M\text{-}O}$ band shifted to a lower frequency, 1000-965 cm^{-1}, from 1035 cm^{-1} while no significant changes was observed in the frequency of $V_{s\ M\text{-}O}$ band. As reported by many investigators (Palomo *et al.*, 1999; Fernandez-Jimenez and Palomo, 2005; Mingyu *et al.*, 2009; Garcia-Lodeiro *et al.*, 2011; Criado *et al.*, 2012), such a shift could be interpreted as representing the formation of amorphous aluminosilicate hydrate gel with alkali-metal ions for charge compensation. It also is possible that Ca liberated from hydrolysis of OPC in hydrothermal environments was part of the gel (N,C-A-S-H) assembled by the interactions between the $Ca(OH)_2$ from OPC, and the aluminosilicate anhydrous compounds like mullite ($3Al_2O_3.\ 2SiO_2$) in FAF at 300°C. The data also revealed that incorporating more OPC into FAF further shifted the $V_{as\ M\text{-}O}$ band to a lower frequency from 1000 cm^{-1} for 90/10 FAF/OPC ratio to 965 cm^{-1} for 80/20 ratio, seemingly suggesting that OPC promoted some changes in the molecular structure of Na_2O- and $CaO\text{-}Al_2O_3\text{-}SiO_2\text{-}H_2O$ (N, C-A-S-H) gel. The other peaks present in these spectra were due to the water ($\delta_{H\text{-}O\text{-}H}$) at 1633 cm^{-1}, CO_3^{2-} ($V_{as\ C\text{-}O}$ and $\delta_{O\text{-}C\text{-}O}$) at 1446 and 876 cm^{-1}, SO_4^{2-} ($V_{s\ S\text{-}O}$) at 1167 cm^{-1}, and quartz ($V_{s\ Si\text{-}O}$ and $\delta_{O\text{-}Si\text{-}O}$) at 798 and 695 cm^{-1}. The similar shift of the $V_{as\ M\text{-}O}$ band to a lower frequency was detected from SMS-, SA-, and SS-activated FAF/OPC cements after autoclaving, reflecting the formation of amorphous alkali metal-, calcium- aluminosilicate hydrate gel, (N, C-A-S-H) gel. This shift to a lower frequency region between 991 and 973 cm^{-1} was more important at higher cement contents (80/20 FAF/OPC ratio). Additionally, there was no noticeable change in the frequency of $V_{s\ M\text{-}O}$ band for both the 80/20 and 90/10 ratio FAF/OPC non-activated blends. The spectra with different alkali activators showed some specific features (Figure 3). Two prominent bands appeared at 1467 and 872 cm^{-1} with SA activator and were assigned to $_{Vas\ C\text{-}O}$ and $\delta_{O\text{-}C\text{-}O}$ in carbonated compounds, while the quartz-associated bands were present at 797 and 694 cm^{-1}. With SS, there were two SO_4^{2-}-related bands at 1165 and 673 cm^{-1} due, respectively, to the $V_{s\ S\text{-}O}$ and $\delta_{o\text{-}s\text{-}o}$, possibly from Ca sulfate (Thompson and Palmer, 1988). In agreement with the XRD results SS activator seemed to inhibit the carbonation reactions of cement; in fact, the carbonation-related bands at 1467 and 872 cm^{-1} were hardly visible. In contrast, the SMS-activated bland showed moderate carbonation. As expected, incorporating more OPC engendered the growth

of carbonate-associated $V_{as\ C\text{-}O}$ and $\delta_{O\text{-}C\text{-}O}$ band peaks at 1458 and 874 cm^{-1} because of the carbonated compounds in the original OPC.
The spectra of non-activated and activated blends before and after the thermal shock closely resembled each other, suggesting that the hydrothermal reaction products (C-A-S-H and N,C-A-S-H gels, and carbonate- and sulfate-compounds), formed by OPC and the activators in cement bodies at 300°C survived the 600°C heat-cool water-quenching thermal-shock test, although decrease in their crystallinity was suggested by the XRD tests.

3.5. Changes in differential thermal gravimetric analyses after the thermal shock (DTG)

Figure 4 presents the results of differential thermal gravimetric analyses before and after the thermal shock for the 80/20 weight ratio blends. Table 4 summarizes the temperatures of the differential weight-loss peaks and the % of mass lost in each temperature interval. The weight loss up to about 400°C can be associated with different hydrates, (calcium, sodium) silica aluminate hydrates, including garronite (Foldvari, 2011), calcium aluminate and calcium silicate hydrates. Between about 400- and 600°C, the dehydration of portlandite occurs along with the weight loss associated with the analcime (Harada *et al.*, 1972); between 600- and 700°C there is decomposition related to carbonates. TGA analysis of the fly ash demonstrated some mass losses between about 700- and 800°C. In the case of the thermal-shock-treated samples, the weight loss associated with carbonates shifted to lower temperatures and was analyzed between 500- and 700°C (Table 4).
There is a general agreement between the DTG, FT-IR and XRD results. Before the thermal shock, the SMS-activated blend revealed the highest weight loss associated with different hydrates, 5.07%, and the none-activated cement the lowest, 3.46%, versus 4.08% and 4.83 % for the SS- and SA- activators, respectively. This is in agreement with the XRD results that showed the largest amorphous phase halo for the SMS-activated sample, suggesting a larger content of amorphous hydrates. Garronite likely contributed to the large dehydration peak of SA-activated blend at ~67°C and the wide peak ~200°C. None of the samples showed dehydration of portlandite, in agreement with the XRD patterns that were free of portlandite peaks. Analcime contributed to the weight loss between 400- and 600-°C; it was the largest loss for the SA-activated sample in agreement with the most intense analcime XRD peaks. The SA-activated sample also had the most important carbonate-decomposition weight loss, 3.65% compared with 1.84% and 1.01% for the SMS- and SS-activated blends respectively, once more supporting findings from the XRD measurements.
After the thermal shock, there were three major changes in the DTG results. The amounts of thermally decomposing phases declined in all three temperature ranges, suggesting fewer water-containing hydrates, analcime, and carbonates. The decomposition temperature of carbonates dropped (the start of the decomposition shifted from about 600- to about 550°C) possibly due to a decrease in their crystallinity. Finally, the broad decomposition peak between about 700- and 800°C attributed to the non-reacted FAF disappeared. The lower amounts of hydrates, analcime, and carbonates after the thermal-shock tests also agree with the results of the XRD analysis.

3.6. Changes in microstructure and elemental composition after thermal shock (SEM/EDX)

Figure 5 shows the micrographs of the FAF/OPC samples alone and with different activators before and after the thermal shock. All the samples contained fly ash cenospheres covered with hydration products and surrounded by irregular, mostly amorphous nodules. Among the three activators, soda ash produced samples with the highest surface roughness. There was no dramatic difference in samples' morphologies after the thermal shock, which, for the most part, remained amorphous.

Elemental analysis showed sites with the composition typical of the CSH gel, tobermorite, garranite, calcium carbonate, riversideite along with quartz, and stand-alone large anhydrate crystals supporting the XRD findings (Table 5). The point 10 denotes the site with the typical composition of wairakite that could not be identified by XRD due to its pattern strongly overlapping with that of analcime. In contrast, crystals of analcime expected from the XRD analysis were not found.

4. Conclusions

Performance of very high-content FAF blends with OPC non-activated or activated with sodium meta silicate, sodium sulfate and soda ash, hydrated at 300°C and subjected to high thermal shock (5 cycles of 600°C heat followed by 25°C water cooling) was evaluated. The following general conclusions can be drawn from the study.

1. The major product of the blend hydration for 24 hours at 85°C followed by 24 hours at 300°C is calcium sodium aluminosilicate hydrate (C,N-A-S-H) gel. More of it forms in activated FAF/OPC blends than in non-activated one leading to their high compression strength. SMS and SA-activators significantly accelerate the hydration of both FAF and OPC. The SA-activator promotes the products' crystallization, while the hydration products of the SMS-activated blend for the most part stay amorphous at early hydration times. SS has the weakest accelerating effect on FAF, likely resulting in delayed FAF hydration in comparison with the OPC.

2. The OPC hydration products, such as small amounts of tobermorite and possibly CSH gel, crystalize in the non-activated blends and in the presence of the SS activator where OPC hydration starts before pozzalan reactions of FAF. The hydrates of sodium calcium aluminum silicate, such as, garronite (SA activator) or wairakite (SMS), along with the FAF-hydration product, analcime, form when OPC and FAF hydrate simultaneously in SA- and SMS-activated blends. Portlandite was not detected in any of the samples. This can be explained by its partial carbonation in the blends with SMS and SA, anhydrate formation in the blend with SS activator, and reactions with FAF with the formation of calcium-containing hydrates.

3. The thermal shock tests reduced the amount of thermally decomposable hydrates and the peak intensities of crystalline products such as garronite and analcime, while tobermorite in non-activated blends survived the tests. In general, the crystallinity of the samples decreased after the thermal shock tests. Although all activators improved the initial compressive strength of the non-activated sample, the compressive strength decreased more than 40- and more than 50% respectively for 80/20-and 90/10 weight ratio blends after the 5 thermal-shock cycles for both activated and non-activated blends.

Acknowledgements

This publication was based on the work supported by the Geothermal Technologies Office in the US Department of Energy (DOE) Office of Energy Efficiency and Renewable Energy (EERE), under the auspices of the US DOE, Washington, DC, under Contract No. DE-AC02-98CH 10886. - 98CH10886.
Research was carried out in part at the Center for Functional Nanomaterials, Brookhaven National Laboratory, which is supported by the U.S. Department of Energy, Office of Basic Energy Sciences, under Contract No. DE-SC0012704.

References

Andini S, Cioffi R, Colangelo F, Grieco T, Montagnaro F, and Santoro L (2008) Coal fly ash raw material for the manufacture of geopolymer-based products. *Waste Management* **28(2)**: 416-423.

Bakharev T (2005) Resistance of geopolymer materials to acid attack. *Cement and Concrete Research* **35(4)**: 658-670.

Bakharev T (2006) Thermal behavior of geopolymers prepared using class F fly ash and elevated temperature curing. *Cement and Concrete Research* **36(6)**: 1134-1147.

Ben Haha M, De Weerdt K, and Lothenbach B (2010) Quantification of the degree of reaction of fly ash. *Cement and Concrete Research* **40(11)**: 1620-1629.

Bentz DP and Ferraris CF (2010) Rheology and setting of high volume fly ash mixtures. *Cement and Concrete Research* **32(4)**: 265-270.

Berry EE, Hemmings RT, and Cornelius BJ (1990) Mechanism of hydration reactions in high volume fly ash pastes and mortars. *Cement and Concrete Composites* **12(4)**: 253-261.

Bignozzi MC, Manzi S, Natali ME, Rickard WDA and van Riessen A (2014) Room temperature alkali activation of fly ash: The effect of Na_2O/SiO_2 ratio. *Construction and Building Materials* **69**: 262-270.

Chi M and Huang R (2013) Binding mechanism and properties of alkali-activated fly ash/slag mortars. *Construction and Building Materials* **40**: 291-298.

Criado M, Fernández Jiménez A, Sobrados I, Palomo A, and Sanz J (2012) Effect of relative humidity on the reaction products of alkali activated fly ash. *Journal of The European Ceramic Society* **32(11)**: (2012) 2799–2807.

Davidovits J (1991) Geopolymers: Inorganic polymeric new materials. *Journal of Thermal Analysis* **37(8)**: 1633-1656.

Deschner F, Winnefeld F, Lothenbach B, Seufert S, Schwesig P, Dittrich S, Goetz-Neunhoeffer F and Neubauer J (2012) Hydration of Portland cement with high replacement by siliceous fly ash. *Cement and Concrete Research* **42(10)**: 1389-1400.

Donatello S, Fernandez-Jimenez A, and Palomo A (2013) Very high volume fly ash cements. Early age hydration study using Na_2SO_4 as an activator. *Journal of American Ceramic Society* **96(3)**: 900-906.

Donatello S, Kuenzel C, Palomo A and Fernandez-Jimenez A (2014) High temperature resistance of a very high volume fly ash cement. *Cement and Concrete Composites* **45**: 234-242.

Donatello S, Palomo A, and Fernandez-Jimenez A (2013) Durability of very high volume fly ash cement pastes and mortars in aggressive solution. *Cement and Concrete Composites* **38**: 12-20.

Duran-Herrera A, Juarez CA, Valdez P and Bentz DP (2011) Evaluation of sustainable high volume fly ash concretes. *Cement and Concrete Composites* **33(1)**: 39-45.

Feldman RF, Carette GG and Malhotra VM (1990) Studies on mechanics of development of physical and mechanical properties of high-volume fly ash-cement pastes. *Cement and Concrete Composites* **12(4)**: 235-251.

Fernandez-Jimenez A and Palomo A (2005) Composition and microstructure of alkali activated fly ash binder: Effect of the activator. *Cement and Concrete Research* **35(10)**: 1984-1992.

Fraay ALA, Bijen JM, de Haan YM (1989) The reaction of fly ash in concrete a critical examination. *Cement and Concrete Research* **19(2)**: 235-246.

Foldvari M (2011) Handbook of thermogravimetric system of minerals and its use in geological practice. In *Occasional Papers of the Geological Institute of Hungary*. Budapest, Hungary, vol. 213.

Harada K, Tanaka K and Nagashima K (1972) New data on the analcime-wairakite series. *American Mineralogist* **57(5-6)**: 924-931.

García-Lodeiro I, Palomo A, Fernández-Jimenez A and Macphee DE (2011) Compatibility studies between N–A–S–H and C–A–S–H gels. Study in the ternary diagram Na2O–CaO–Al2O3–SiO2–H2O. *Cement and Concrete Research* **41(9)**: 923–931.

Ghosh SN and Handoo SK (1980) Infrared and Raman spectral studies. *Cement and Concrete Research* **10(6)**: 771-782.

Gill SK, Pyatina T, and Sugama T (2012) Thermal shock-resistant cement. *Geothermal Resources Council Transactions* **36**: 445-451.

Gunasekaran S, Anbalagan G, and Pandi S(2006) Raman and infrared spectra of carbonate of calcite structure. *Journal of Raman spectroscopy* **37(9)**: 892-899.

Gurney L, Bentz DP, Sato T and Weiss WJ (2012) Reducing set retardation in high volume fly ash mixtures with the use of limestone: Improving constructability of sustainability. In *Transportation Research Record, Journal of the Transportation Research Board*, No. 2290, Concrete Materials 139-146.

Joshi SV and Kadu MS (2012) Role of alkali activator in development of eco-friendly fly ash based geopolymer concrete. *International Journal of Environmental Science and Development* **3**: 417-421.

Kline AA and Mullins ME (1991) Sol-gel kinetics followed by cylindrical attenuated total reflectance infrared spectroscopy. *Journal of the American Ceramic Society* **74(10)**: 2559-25563.

Komnitsas K and Zaharaki D (2007) Geopolymerization: A review and prospects for the minerals industry. *Minerals Engineering* **20(14)**: 1261-1277.

Lam L, Wong YL and Poon CS (2000) Degree of hydration and gel/space ratio of high-volume fly ash/cement systems. *Cement and Concrete Research* **30(5)**: 747-756.

Lohani TK, Jena S, Dash KP and Padhy M (2012) An experimental approach on geopolymer recycled concrete using partial replacement of industrial byproduct. *International Journal of Civil and Structural Engineering* **3**: 141-149.

Mandal S and Majumdar D (2009) Study on the alkali activated fly ash mortar. *The Open Civil Engineering Journal* **3**: 98-101.

Mingyu H, Xiaomin Z and Fumei L (2009) Alkali-activated fly ash-based geopolymer with zeolite or bentonite as additives. *Cement and Concrete Composites* **31(10)**: 762–768.

Pacewska B and Wilinska I (2013) Hydration of cement composites containing large amount of waste materials. *Procedia Engineering* **57**: 53-62.

Palomo A, Grutzeck MW and Blanco MT (1999) Alkali-activated fly ashes A cement for the future. *Cement and Concrete Research* **29(8)**: 1323-1329.

Ramasamy V and Suresh G (2009) Mineral characterization and crystalline nature of quartz in Ponnaiyar river sediments, Tamilnadu, India. *American-Eurasian Journal of Science Research* **4(2)**: 103-107.

Rodriguez ED, Bernal SA, Provis JL, Paya J, Monzo JM and Borrachero MV (2013) Effect of nano silica-based activators on the performance of an alkali-activated fly ash binder. *Cement and Concrete Composites* **35(1)**: 1-11.

Saikia BJ, Parthasarathy G and Sarmah NC (2008) Fourier transform infrared spectroscopic estimation of crystallinity in SiO2 based rocks. *Bulletin of Material Science* **31(5)**: 775-779.

Shi C and Day RL (1995) Acceleration of the reactivity of fly ash by chemical activation. *Cement and Concrete Research* **25(1)**: 15-21.

Thompson MM and Palmer RA (1988) In situ Fourier transform infrared diffuse reflectance and photoacoustic spectroscopy characterization of sulfur-oxygen species resulting from the reaction of SO_2 with $CaCO_3$. *Applied Spectroscopy* **42(6)**: 945-951.

Uchino T, Sakka T and Iwasaki M (1991) Interpretation of hydrated states of sodium silicate glasses by infrared and Raman analysis. *Journal of American Ceramic Society* **74(2)**: 306-313.

van Jaarsveld JGS, van Deventer JSJ and Lukey GC (2002) The effect of composition and temperature on the properties of fly ash- and kaolinite-based geopolymers. *Chemical Engineering Journal* **89 (1-3)**: 63-73.

Xyla AG and Koutsoukos PG (1989) Quantitative analysis of calcium carbonate polymorphs by infrared spectroscopy. *Journal of Chemical Society, Faraday Trans.1* **85(10)**: 3165-3172.

Ylmen R and Jaglid U (2013) Carbonation of Portland cement studied by diffuse reflection Fourier transform infrared spectroscopy. *International Journal of Concrete Structures and Materials* 7(**2**): 119-125.

Tables

Table 1. Oxide composition of ordinary Portland cement (OPC), Fly Ash F (FAF) and Sodium Meta-silicate (SMS) used in the study.
Table 2. Compressive strength of specimens before and after 5 thermal-shock cycles.
Table 3. Crystalline phase composition of specimens before and after 5 thermal-shock cycles.
Table 4. Thermal decomposition temperature ranges and associated weight losses of specimens before and after 5 thermal-shock cycles.

Figures

Figure 1. Normalized heat released at 25°C during hydration of 80/20 weight ratio FAF/OPC blend activated with SA (a), SMS (b), SS (c) and non-activated (d)
Figure 2. X-ray diffractograms for 80/20 weight ratio FAF/OPC specimens before (top) and after (bottom) activated 5 thermal-shock cycles with SA (a), SMS (b), SS (c) and non-activated (d); 1-quartz, 2-mullite, 3-hematite, 4-tobermorite, 5-calcite, 6-anhydrate, 7-analcime, 8-garronite, 9-riversideite
Figure 3. Fourier transform infrared spectra of 80/20 weight ratio blend before (top) and after 5 thermal-shock cycles (bottom) activated with SA (a), SMS (b), SS (c) and non-activated (d)
Figure 4. Differential thermal gravimetric analyses (DTG) of 80/20 weight ratio blend before (top) and after (bottom) 5 thermal-shock cycles activated with SA (a), SMS (b), SS (c) and non-activated (d)
Figure 5. Scanning electron micrographs of typical cement microstructures and their elemental compositions for 80/20 and 90/10 weight ratios FAF/OPC blends

Table 1
Click here to download Table: Pyatina-Table 1.docx

Component	Al_2O_3	CaO	SiO_2	Fe_2O_3	Na_2O	K_2O	TiO_2	SO_3
OPC, Type II cement, atomic %	2.9	66	18	3.8	0.34	1.3	-	5.4
Fly ash class F, atomic %	35	2.7	50	7.1	0.30	3.1	1.6	-
Sodium meta silicate, wt.%	-	-	46.6	-	50.5	-	-	-

Table 2
Click here to download Table: Pyatina-Table 2.docx

Activator	Compressive strength, MPa		% Compressive Strength Decrease
	Before thermal shock	After thermal shock	
	80/20 % by weight FAF/OPC		
No activator	17	8.9	47
SMS	19	9.7	49
SA	17	9.2	43
SS	20	11	46
	90/10 % by weight FAF/OPC		
No activator	8.7	4.2	51
SMS	12.0	5.9	51
SA	12	4.7	59
SS	13	8.8	34

Table 3
Click here to download Table: Pyatina-Table 3.docx

Specimen	Before thermal shock		After thermal shock	
	Major phases	Minor phases	Major phases	Minor phases
No activator	quartz (SiO_2), mullite ($3Al_2O_3 \cdot 2SiO_2$), hematite (Fe_2O_3), calcite $CaCO_3$	Tobermorite-11A $Ca_5(OH)_2Si_6O_{16} \cdot 4H_2O$, CSH (I) $CaO \cdot SiO_2 \cdot H_2O$, Gypsum $CaSO_4 \cdot 2\ H_2O$	quartz (SiO_2), mullite ($3Al_2O_3 \cdot 2SiO_2$), hematite (Fe_2O_3), calcite $CaCO_3$	Tobermorite-11A $Ca_5(OH)_2Si_6O_{16} \cdot 4H_2O$, CSH (I) $CaO \cdot SiO_2 \cdot H_2O$ Gypsum $CaSO_4 \cdot 2\ H_2O$
SMS	quartz (SiO_2), mullite ($3Al_2O_3 \cdot 2SiO_2$), hematite (Fe_2O_3), analcime $Al_2O_3 \cdot Na_2O \cdot 4SiO_2 \cdot 2H_2O$, calcite $CaCO_3$	Riversideite (tobermorite-9A) $Ca_5Si_6O_{16}(OH)_2$	quartz (SiO_2), mullite ($3Al_2O_3 \cdot 2SiO_2$), hematite (Fe_2O_3), calcite $CaCO_3$	analcime $Al_2O_3 \cdot Na_2O \cdot 4SiO_2$
SS	quartz (SiO_2), mullite ($3Al_2O_3 \cdot 2SiO_2$), hematite (Fe_2O_3), anhydrate $CaSO_4$ calcite $CaCO_3$	Tobermorite-11A $Ca_5(OH)_2Si_6O_{16} \cdot 4H_2O$	quartz (SiO_2), mullite ($3Al_2O_3 \cdot 2SiO_2$), hematite (Fe_2O_3), Anhydrate $CaSO_4$ calcite $CaCO_3$	Tobermorite-11A $Ca_5(OH)_2Si_6O_{16} \cdot 4H_2O$
SA	quartz (SiO_2), mullite ($3Al_2O_3 \cdot 2SiO_2$), hematite (Fe_2O_3), garronite $NaCa_{2.5}(Al_6 Si_{10})O_{32} \cdot 14H_2O$, analcime $Al_2O_3 \cdot Na_2O \cdot 4SiO_2 \cdot 2H_2O$, calcite $CaCO_3$		quartz, mullite, hematite, calcite	analcime $Al_2O_3 \cdot Na_2O \cdot 4SiO_2$, garronite $NaCa_{2.5}(Al_6 Si_{10})O_{32} \cdot 14H_2O$

Table 4
Click here to download Table: Pyatina-Table 4.docx

Activator	Before the thermal shock			After the thermal shock		
	70-400 °C	400-600 °C	600-700 °C	70-400 °C	400-500 °C	500-700 °C
	80/20 FAF/OPC					
None	3.46	1.33	1.08	1.70	0.13	0.24
SMS	5.07	1.61	1.84	2.79	0.33	1.60
SS	4.08	1.51	1.01	1.90	0.25	0.78
SA	4.83	2.22	3.65	2.29	0.46	3.79

Figure 1
Click here to download Figure: Pyatina-Figure 1.tif

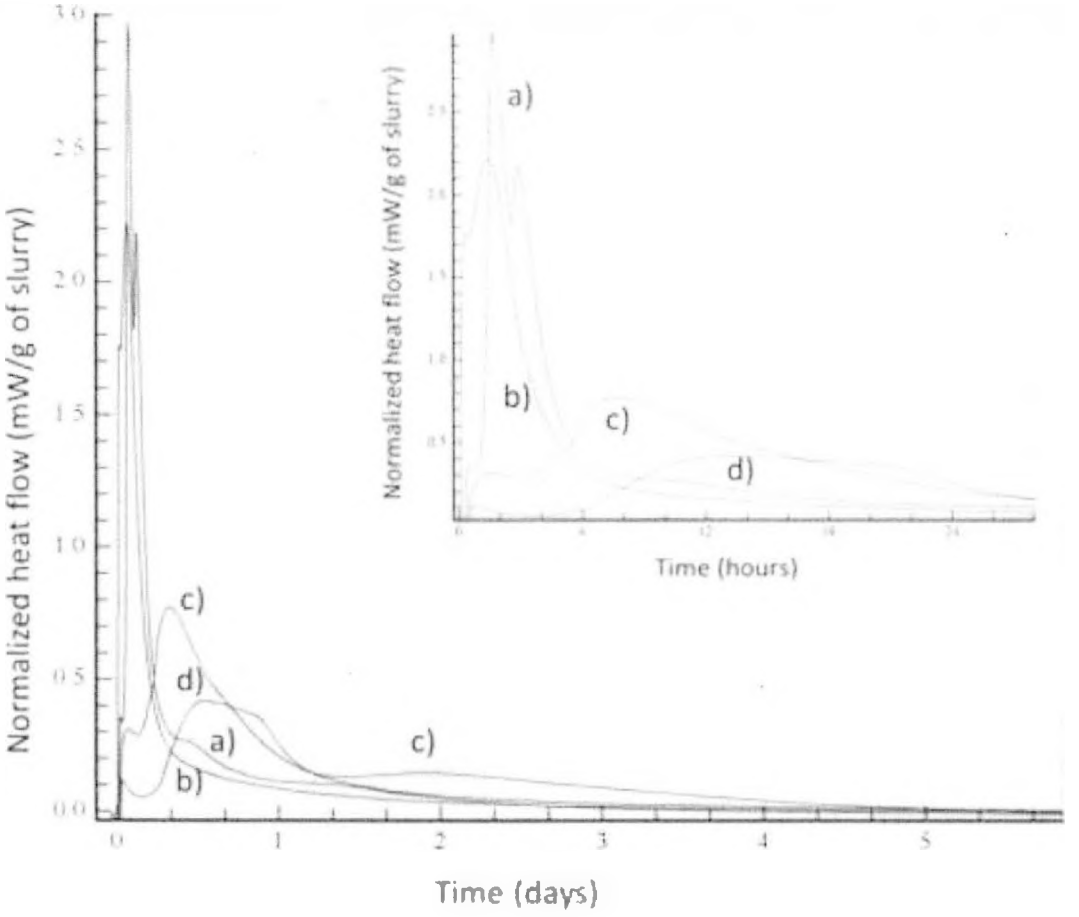

Figure 2
Click here to download Figure: Pyatina-Figure 2.tif

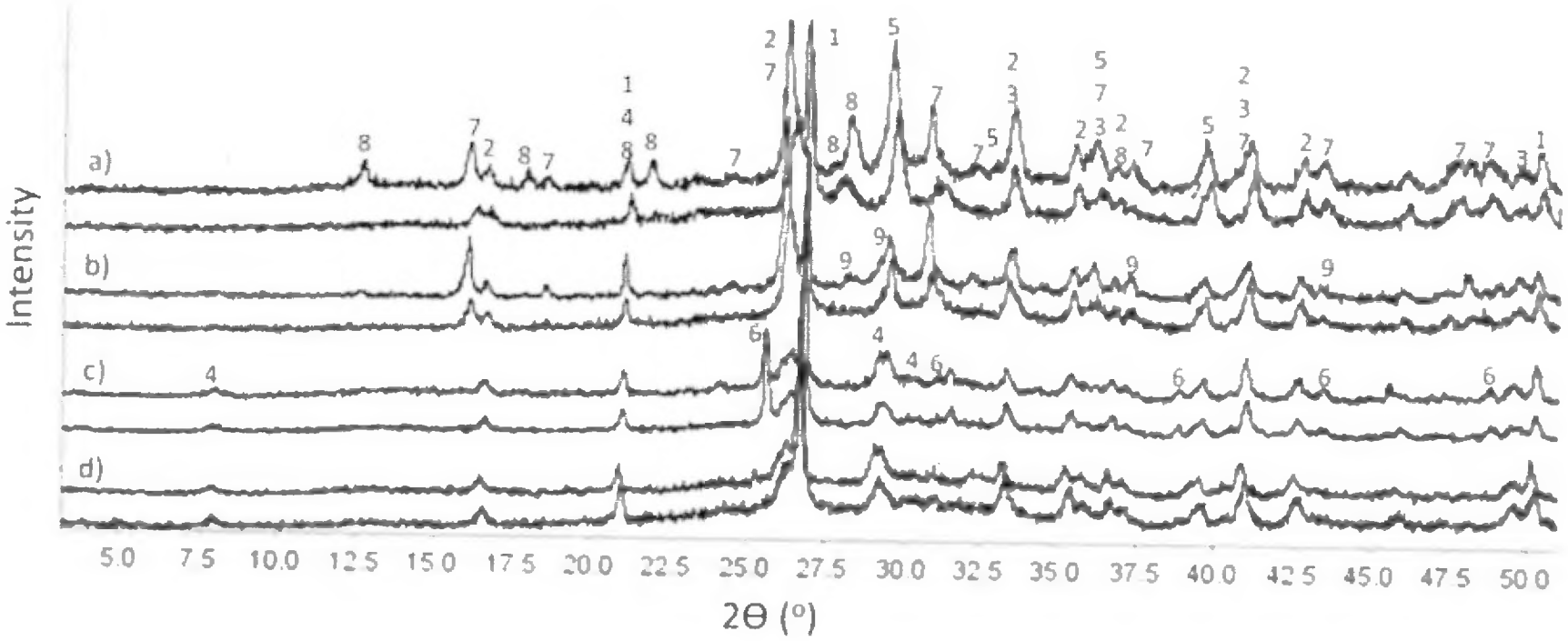

Figure 3
Click here to download Figure: Pyatina-Figure 3.tif

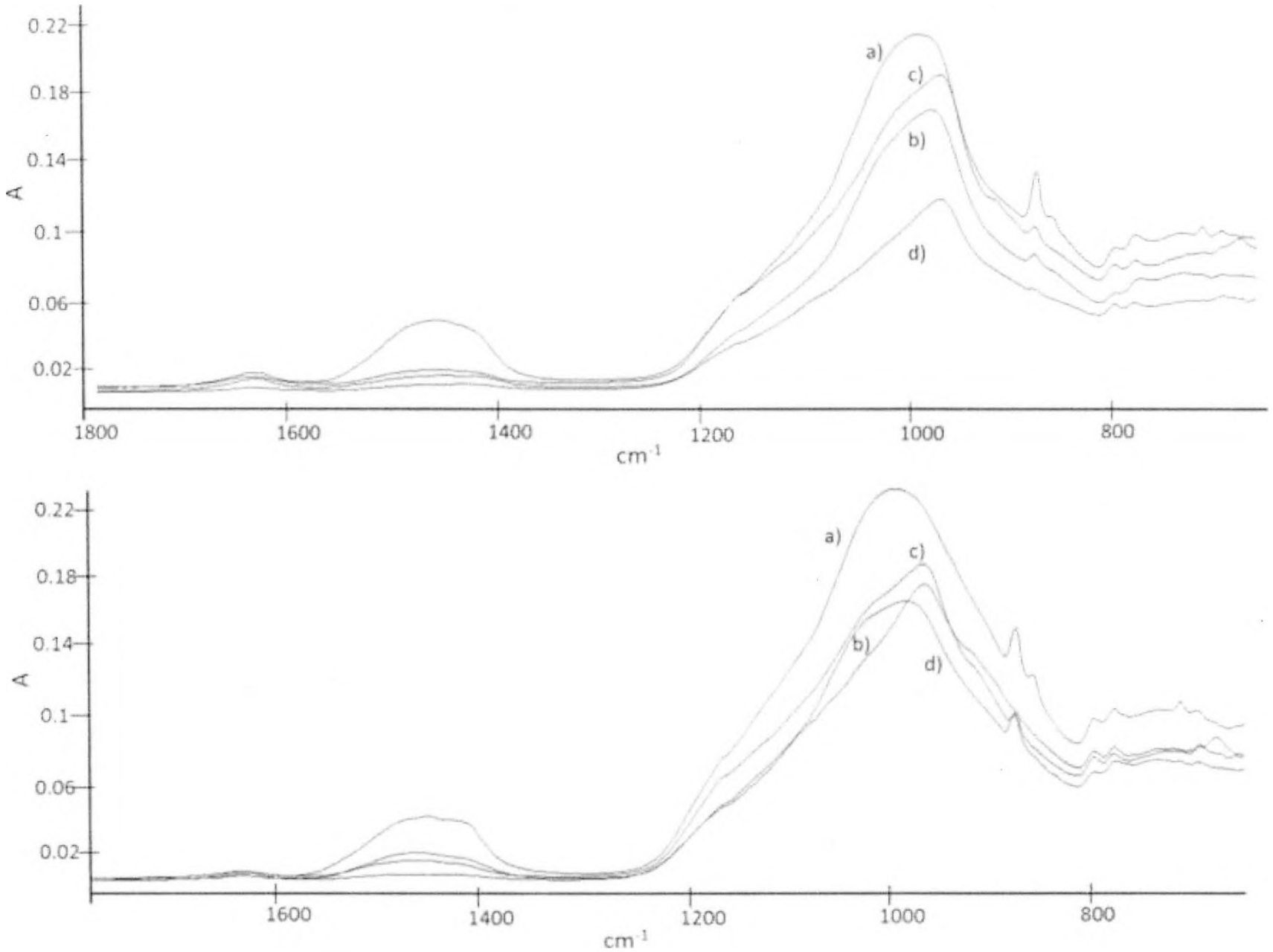

Figure 4
Click here to download Figure: Pyatina-Figure 4.tif

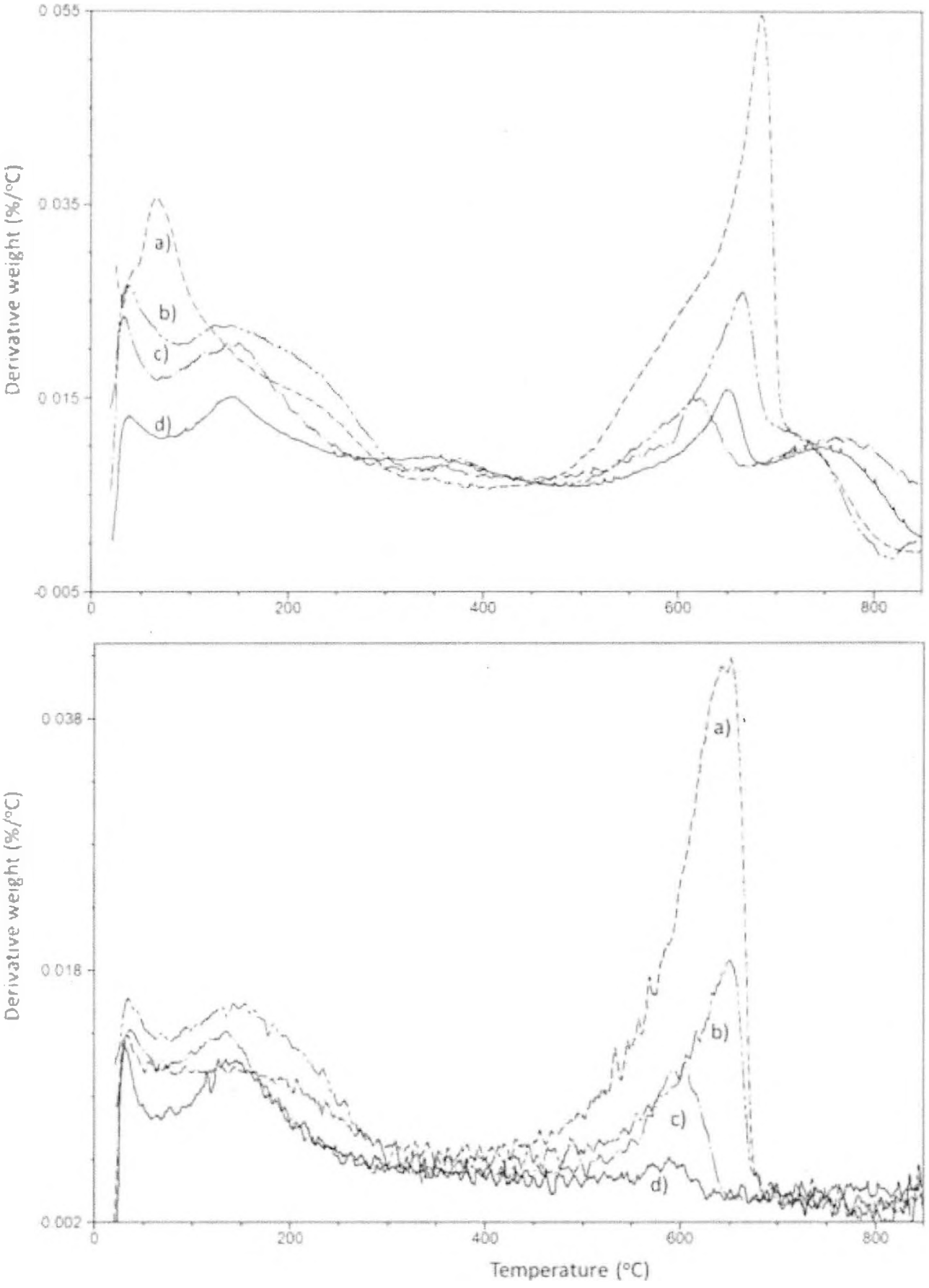

Figure 5
Click here to download Figure: Pyatina-Figure 5.tif

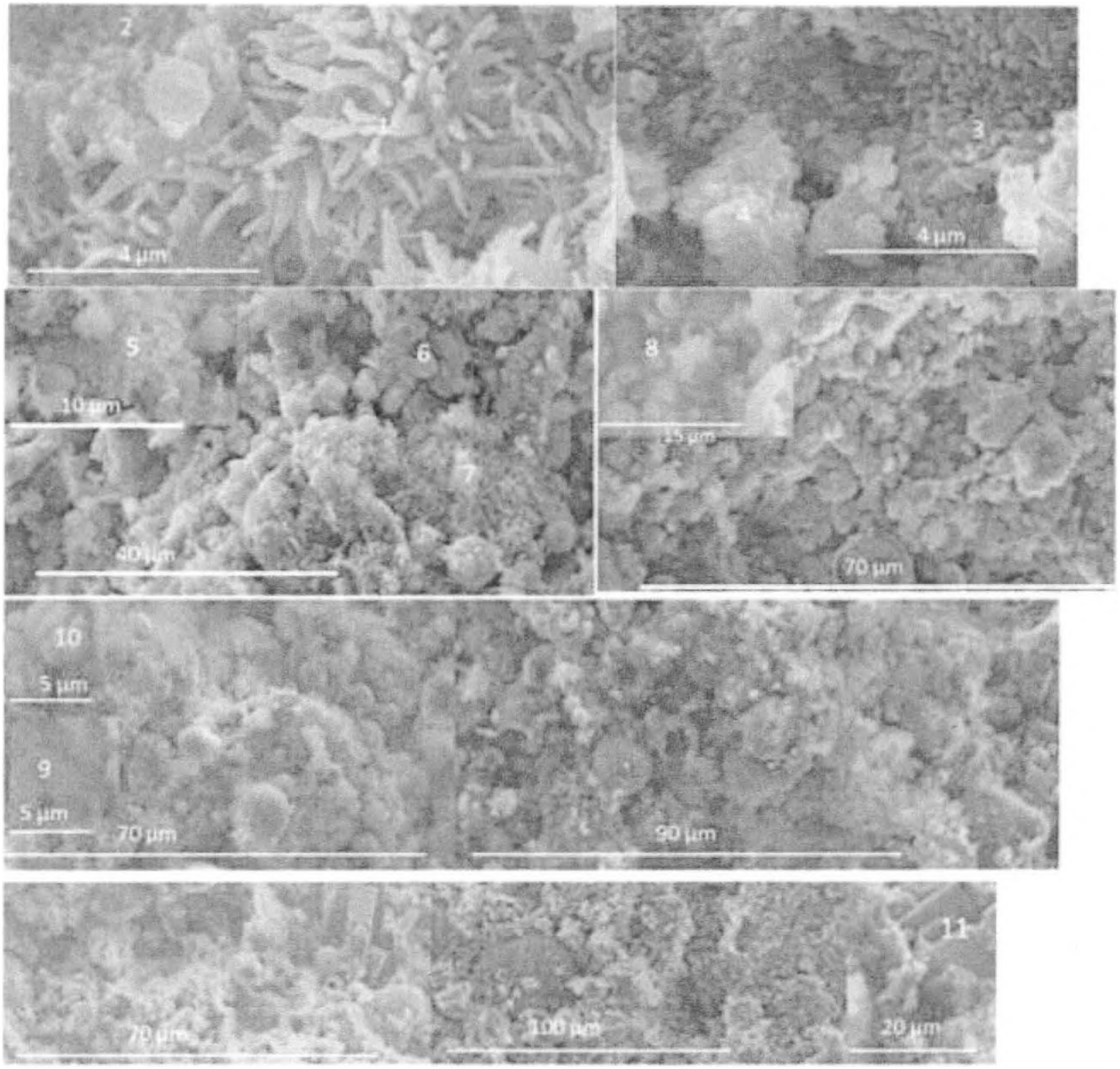

Sample	Point	Al	Ca	K	Na	Si	S	Possible phase
80/20 before TS	1	3.8	19	1.8	-	15	-	CSH
	2	4.2	15	1.6	-	18	-	Tobermorite
80/20 after TS	3	2.1	12	1.1	0.1	11	-	CSH
	4	2.3	4.8	0.6	0.4	8.9	0.6	-
90/10-SA-before TS	5	5.1	16	0.9	2.5	16	-	CSH (precursor)
	6	9.5	4.5	1.7	1.2	19	-	Garronite
	7	11	5.1	-	2.6	20	-	Garronite
90/10-SA-after TS	8	6.4	2.7	1.0	1.0	12	-	Garronite
90/10-SMS-before TS	9	5.5	12	3.3	0.8	15	-	Riversideite (precursor)
	10	10	3	1	2	19	-	Wairakite (precursor)
80/20 – SS-after TS	11	0.1	12	-	-	0.2	13	Anhydrate